Nanoscale

PAPER

View Article Online
View Journal | View Issue

Cite this: *Nanoscale*, 2025, **17**, 5993

Magnetic nanoparticle-based hydrogels as reliable platforms to investigate magnetic interactions†

I. Morales, *[a,b,c] A. Koch, [b] C. Wesemann, [b,d] R. T. Graf [b,c,d] and N. C. Bigall *[c,e,f]

Received 16th October 2024,
Accepted 27th January 2025

DOI: 10.1039/d4nr04286g

rsc.li/nanoscale

In this work we design and synthesize magnetic nanoparticle-based hydrogels in which the inter-particle dipolar interactions can be tailored within the networks. These emerging materials combine the porosity and high surface area characteristic of gels with the nanoscopic magnetic properties of the building blocks, all in one macroscopic material. The synthesis of self-supported magnetic nanocrystal-based hydrogels is done through an amphiphilic overcoating and gelation procedure. The control over the dipolar interactions within the nanoparticles and aggregates forming the hydrogel network is achieved by changing the length of the hydrophobic side chain of the amphiphilic polymer used to coat and water transfer the nanoparticles. A scale-up approach of the overcoating procedure is presented. As well, we demonstrate that these systems are very useful to study, understand and easily tailor the magnetic interactions between particles or aggregates, in a more controlled and reliable way than in the nanoparticle colloids.

Introduction

The assembly of inorganic nanoparticles (NPs) into macroscopic self-supported porous networks, either hydrogels or aerogels, constitute a new interesting type of materials characterized by their open porous structure, large specific surface area and very low density.[1–3] These properties make them promising for different applications such as catalysis, sensing, energy harvesting, environmental remediation and biomedicine.[4–7] Moreover, these materials can preserve the nanoscopic properties of their building blocks at the macroscale or showcase collective properties not present in the bulk neither in the nanocrystals alone.[3,8,9]

For the fabrication of nanoparticle-based gels, the NP colloids must be destabilized avoiding an uncontrolled NP agglomeration. To do this, it is mandatory to manipulate the interparticular forces by either attenuating the repulsive forces between the NPs or introducing controlled attractive forces.[10] The strategy to follow will depend, among other parameters, on the dispersing medium of the NPs (*i.e.* polar or non-polar solvent) and their surface functionalization. In general terms, the destabilization can be done either *via* progressive removal of ligands (*e.g.* oxidation) or ionic cross-linking.[11,12] Interestingly, reversible NP assemblies can also be achieved by means of dynamic covalent bonding,[13] highlighting the versatility and possibilities of NP gelation to engineer new functional materials. As a result, highly porous gels are obtained, which are frequently called solvogels when the pores are filled with a solvent. If the solvent is water, they are known as hydrogels. Afterwards, different drying procedures can be used to replace the solvent in the pores with air without producing the network destruction, yielding the so-called aerogels.[2]

In particular, magnetic nanoparticle-based gels are of special interest because it is possible to synergistically exploit the nanoscopic magnetic properties of the MNP building blocks (*e.g.* superparamagnetism, heating upon application of radiofrequency fields...) with that of the gels and they can be manipulated by external magnetic fields.[14,15] In spite of the enormous potential of MNP-based gels, most of the studies to date are mainly done by dispersing MNPs into silica, alumina, carbon or polymeric matrices,[16–20] rather than having the synthesized MNPs networked together to form self-supporting structures. Nevertheless, in the last years, increased attention has been devoted to these materials and to the study of their magnetic properties.[21–26] In the work of Hettiararchchi *et al.*,[21]

[a]*Institute of Inorganic Chemistry, Leibniz University Hannover, Callinstraße 9, 30167 Hannover, Germany. E-mail: irene.morales@aca.uni-hannover.de*
[b]*Institute of Physical Chemistry and Electrochemistry, Leibniz University Hannover, Callinstraße 3a, 30167 Hannover, Germany*
[c]*Cluster of Excellence PhoenixD (Photonics, Optics and Engineering- Innovation Across Disciplines), Leibniz University Hannover, 30167 Hannover, Germany*
[d]*Laboratory of Nano and Quantum Engineering, Leibniz University Hannover, Schneiderberg 39, 30167 Hannover, Germany*
[e]*Institute of Physical Chemistry, University of Hamburg, Grindelallee 117, D-20146 Hamburg, Germany. E-mail: nadja-carola.bigall@uni-hamburg.de*
[f]*The Hamburg Centre for Ultrafast Imaging, Hamburg, Germany*
† Electronic supplementary information (ESI) available. See DOI: https://doi.org/10.1039/d4nr04286g

the authors report the aerogelation of $Fe_{1.3}Ni_{0.7}P$ nanorods *via* oxidation-induced gelation, in which they did not observe any remarkable difference between the magnetic properties of the NP colloids and the aerogels thereof. On the other hand, Berestok *et al.*[22] synthesized maghemite aerogels and briefly investigated the magnetic properties, suggesting that the random NP interconnection in the aerogel network has an impact in the overall magnetic properties. As well, in our recent work on FePt and $CoPt_3$ aerogels,[24] we thoroughly investigated the effect of the gelation process and aerogel structure on the magnetic properties, reporting that the closer contact of the NPs in the gel network produces changes in the magnetic properties of the aerogels compared to the NP colloids.

Despite these interesting works regarding magnetic aerogels, up to date, a detailed investigation of the magnetic interactions between the nanoparticles within a hydrogel network and its influence in the overall properties has not been done, neither the investigation on how to smart tune the magnetic properties of these materials. The understanding of the effect of dipolar interactions into the overall magnetic properties of nanoparticulate systems[27,28] is of outmost importance for several applications. In the case of magnetic hyperthermia, for example, the nanoparticle concentration and their local aggregation have an impact on the interaction between the nanoparticles, producing an increase or decrease of the heating efficiency,[29–33] which in most cases is very difficult to control or anticipate. The versatility and possibilities given by the gelation strategies available can lead to structures in which the interactions between the nanoparticles can be controlled and tuned, obtaining systems with or without direct contact between the nanoparticle interfaces, in which the dipole–dipole interactions can be modified by changing the distance between the NPs or their arrangement. As well, collective properties can arise from the network itself, due to the interactions and coupling between the NPs in the assembly.

Here, we demonstrate that magnetic nanoparticle-based hydrogels are excellent platforms to investigate and fine tune interactions between particles in a more reliable and controlled way than in colloids, which has not been previously reported on hydrogels. We fabricate iron oxide nanoparticle (IONP) hydrogels in which the inter-particle interactions are tuned, following our previously reported amphiphilic polymer-coating and gelation procedure.[26] For that, IONPs are synthesized in organic media and water transfer by means of poly(isobutylene-alt-maleic anhydride) (PMA) modified with 1-dodecylamine following the procedure of Lin *et al.*,[34] or with the shorter *n*-octylamine as side-chain. We propose the use of these hydrophobic side-chain lengths (octylamine *vs.* dodecylamine) to be able to finely control the distance between the NPs within the networks and therefore, their dipolar interactions and the collective properties of the hydrogels. Indeed, the choice of octylamine and dodecylamine ligands will give rise to different scenarios. In the first case, the increased interparticle interactions could enhanced the heating efficiency of the systems, beneficial for magnetic hyperthermia, while in the latter no changes are expected upon gelation due to higher distances between the nanoparticles, giving rise to more stable and robust systems against aggregation, useful for the fabrication of sensors or actuators. Furthermore, we perform a systematic investigation into how varying the amount of polymer used to coat the NPs affects both their hydrodynamic size and the magnetic properties of the resulting NP colloids and hydrogels. We also present an easy way to scale-up the polymer-coating with PMA-1-dodecylamine. Our findings highlight the critical role of interparticle interactions in governing the collective behavior of magnetic nanoparticles within porous soft matter macroscopic systems.

The gelation is done *via* the addition of Ca^{2+} ions which destabilize the aqueous colloidal NPs and bridge the NPs together through the carboxylic acid moieties present in the polymer shell, creating the NP network. The versatility of this procedure to aerogelate any shape or composition NP, avoiding undesired changes in the NP properties (due to ligand removal usually involved in the water transfer of the NPs from organic media), was demonstrated in our previous work.[26] As well, we briefly investigated the properties of an IONP aerogel coated with PMA-1-dodecylamine, where no difference in the magnetic properties (mainly in the magnetic saturation) was observed with respect to the NPs colloids. However, the study of the magnetic properties of the hydrogels as well as the influence of the side-chain length into the magnetic properties has not been researched yet.

Summarizing, achieving a precise and reliable control and understanding of the magnetic interactions is desired to assure a good performance of MNPs, for example, in inductive heating applications. Thus, in this work we propose and systematically investigate novel platforms based on iron oxide nanoparticle hydrogels in which the magnetic properties and magnetostatic interactions between the nanoparticles within the gels can be controlled.

Experimental methods

Chemicals

All chemicals were used without further purification. Poly(isobutylene-*alt*-maleic anhydride) with an average M_w 6000, 12–200 mesh (85%) from Sigma Aldrich, tetrahydrofuran (THF 99.9%, Roth), dodecylamine (98% Sigma Aldrich), 1-octylamine (99% Sigma Aldrich), oleylamine (OAm) with a C18 content of 80%–90% (ThermoFischer), acetone (≥99.5% Sigma Aldrich), ethanol (≥99.8% Sigma Aldrich), hexane (99% Honeywell), chloroform (≥99% Honeywell), iron pentacarbonyl ($Fe(CO)_5$ 99.99% Sigma Aldrich), *n*-octylether (99% Sigma Aldrich), oleic acid (90% Sigma Aldrich), oleylamine (OAm 90% Sigma Aldrich), trimethylamine-*N*-oxide (TMANO 95.5% Sigma Aldrich), sodium hydroxide (≥99% Roth), calcium nitrate tetrahydrate (≥99% Roth), milliQ water (18.2 MΩ cm, from Sartorius water system).

Synthesis of the iron oxide nanoparticles (IONPs)

Maghemite nanoparticles have been synthesized by scaling up the procedure from Hyeon *et al.*,[35] *via* thermal decomposition of iron pentacarbonyl in the presence of oleic acid and sub-

sequent controlled oxidation using trimethylamine oxide. In detail, for the synthesis of 5 nm IONPs, a mixture of 60 mL of octyl ether and 5.81 g of oleic acid was prepared into a 100 mL three neck round bottom flask and degassed and stirred under vacuum for 15 min. After that, the flask was flushed with argon and the mixture was heated to 130 °C. Then, 1.2 mL of $Fe(CO)_5$ were rapidly injected and the mixture was heated to reflux (~280 °C) and kept at that temperature for 1 h. The resulting solution was cooled down to room temperature, and 2.04 g of $(CH_3)_3NO$ (TMANO) were added. The temperature was increased again under argon atmosphere to 130 °C and kept for 2 h. After that, the reaction temperature was increased slowly (3 °C min^{-1}) to reflux and kept at that temperature for another hour. The mixture was cooled down to room temperature and washed with 20 mL of a previously prepared 1 : 1 ethanol/hexane (v/v) and centrifuging at 10 000 rcf (relative centrifugal force) during 15 min. The supernatant was removed and the cleaning procedure was repeated three times by adding 20 mL of 1 : 1 ethanol/hexane (v/v) on each round. Finally, the resulting black precipitate was redispersed in hexane.

Synthesis of the amphiphilic polymers

The amphiphilic polymers were synthesized using the procedure of Lin *et al.*[34] with some modifications. The polymers are based on poly(isobutylene-*alt*-maleic anhydride) backbone, named PMA, and alkylamines as hydrophobic side-chains. In this work, two different side-chains with different lengths have been used, dodecylamine and *n*-octylamine, in order to tailor the interparticle distances of the magnetic nanoparticles and therefore their interactions.

Synthesis of the polymer with dodecylamine (PMA-Dod). The precursor polymer PMA (3.084 g, 20 mmol monomer) was dissolved under magnetic stirring in 80 mL anhydrous tetrahydrofuran (THF) to assure the activity of the maleic anhydride rings. The solution was heated to 60 °C. Once the temperature was reached, 2.86 g of 1-dodecylamine were dissolved in 20 mL of THF, added to the heated THF solution and stirred for 3 h. The solution was transferred to a one-neck flask (V_{flask} = 500 mL) and reduced to a third of the original volume using a rotary evaporator (Heidolph Hei-VAP). For that, the temperature of the rotary evaporator water bath was settled to 50 °C and 90 rpm and the pressure was reduced from 450 mbar to a minimum of 320 mbar. After partial removal of the solvent, the solution was transferred back into a three-neck flask (V_{flask} = 100 mL) and stirred for another 3 h at 60 °C. The final polymer was obtained by transferring the solution to a one-neck flask (V_{flask} = 100 mL) and removing the entire solvent by using the rotary evaporator. After all the solvent was evaporated, 40 mL of chloroform was added to redisperse the polymer by using an ultrasonic bath, obtaining a transparent solution. The amount of dodecylamine added corresponds to 75% with respect to the monomer units and the final polymer concentration in the 40 mL chloroform stock solution is 0.5 M with respect to the monomer units.

Synthesis of the polymer with *n*-octylamine (PMA-Oct). A similar procedure was followed to synthesize the amphiphilic polymer with a shorter alkylamine (*n*-octylamine). 3.04 g of PMA were dissolved in 80 mL THF and heated to 60 °C under vigorous magnetic stirring. Then, 2.53 mL of *n*-octylamine in 25 mL THF were added. This amount is chosen to have the same molarity as in the case of the dodecylamine. The solution was stirred for 3 h at 60 °C and transferred to a one neck flask to reduce the volume to one third of the initial volume. Then, the solution was transferred into a three-neck flask, heated to 60 °C and stirred for another 3 h. The product was transferred to a one neck flask and left overnight to remove the solvent using a rotary evaporator. As in the previous synthesis, the final polymer was dispersed in 40 mL chloroform by using ultrasonic bath.

In both cases, the polymer concentration reached was 0.5 M with respect to the monomer units. The reaction took place at molar ratio of 1 : 0.75 (PMA/alkyl chain) and therefore 25% of the maleic anhydride rings were kept intact, allowing additional modifications if desired.

Polymer coating of the IONPs and water transfer

This procedure is adapted[26,34] with some modifications as described in the following. The synthesized IONPs were sonicated for 5 min before further use. For each coating, 300 μL nanoparticle suspension ([γ-Fe_2O_3] = 18.8 mg mL^{-1}) was filled into a 1.5 mL Eppendorf, 1 mL ethanol was added and it was centrifuged for 5 minutes at 11 000 rcf and the supernatant was discarded. The precipitate was redispersed in 100 μL chloroform by using ultrasonic bath. Then, the desired amount of the polymer stock solution (volumes ranging from 100 μL to 3 mL) was put into a glass vial and the 100 μL iron oxide nanoparticles in chloroform were added. It is important to notice that always the same amount of iron oxide nanoparticles was added, only changing the polymer amount. For the coating with magnetic stirring, the mixture was vigorously stirred keeping the vial open until complete evaporation of the chloroform. For the coating by ultrasonication, the mixture of the polymer and the nanoparticles was sonicated in an open vial at maximum power until all the solvent was evaporated.

Once the solvent was evaporated, each sample was dispersed in 10 mL 0.1 M NaOH by using an ultrasonic bath. In all cases this step was accomplished after no more than 5 min of sonication. Then, the coated iron oxide nanoparticles were filtered through a syringe filter (Millipore Millex-GP PES with 0.22 μm pore size). To exchange the alkaline solution previously added to MilliQ water (18.2 MΩ cm), the filtered nanoparticles were transferred into centrifugal filter units (molecular weight cutoff, MWCO = 30 000) and centrifuged at 3770 rcf for 5 minutes. The transparent and clear supernatant on the bottom of the filter tube was discarded and Milli-Q water was added. The procedure was repeated 5 times. All the nanoparticles coated with different amounts of polymer, independently of the alkyl chain length, were stable in MilliQ water. Finally, to clean the excess of unreacted polymer micelles present in the samples, ultracentrifugation was per-

formed at 100 000*g* and 21 °C during 1 h (twice). After the first hour, the completely transparent supernatant was removed and MilliQ water was added. Finally, all the supernatant was removed and the samples were redispersed in 2 mL of MilliQ water to assure that all the samples remained with the same concentration. The ultracentrifuge used was a Beckman Coulter using a fixed angle rotor Typ 70 Ti (8X39 mL), located in the Centre of Biomolecular Drug Research (BMWZ-LUH).

Scaling up of the polymer-coating strategy

For the scale up, 3 mL of γ-Fe_2O_3 nanoparticles ([γ-Fe_2O_3] = 18.8 mg mL^{-1}) in hexane were centrifuged to remove the solvent and to exchange it with 1 mL of chloroform. In an open one neck round bottom flask, 4 mL of the stock polymer solution (PMA-Dod) and the magnetic nanoparticles in chloroform were added and magnetically stirred at 330 rpm during roughly 2 h. To remove the remaining solvent, the rotary evaporator was operated at 50 °C, 90 rpm and the pressure reduced from 450 mbar to a minimum of 320 mbar. The resulting highly viscous coated nanoparticles were easily dispersed in 100 mL 0.1 M NaOH within a few minutes of ultrasonication. After that, the same filtering and ultracentrifugation steps as explained before were carried out and finally, the nanoparticles were redispersed in 10 mL of MilliQ water.

Hydrogelation of the polymer-coated IONPs

The hydrogels were prepared in Eppendorf tubes by adding 8 μL of a 2 M $Ca(NO_3)_2$ solution to 300 μL of the cleaned coated iron oxide nanoparticles. The addition of the divalent ions causes the controlled destabilization of the nanoparticles and the gelation. The gelation took place overnight. To wash the gels, the thin transparent supernatant layer on top of the hydrogel was removed and 1 mL of MilliQ water was added carefully to preserve the hydrogel structure. This is repeated 5 times each day during two consecutive days to obtain the final hydrogels. It is worth to mention that these self-supported nanoparticle-based hydrogels are usually very brittle. Nevertheless, in all cases, it is possible to wash and handle them without affecting or breaking the network. All the washed hydrogels are stable in water for at least 1 year, with no change in their volume (no further shrinkage) or in their macroscopic shape.

Instrumentation

Dynamic light scattering (DLS) measurements. DLS was performed in a Malvern Panalytical Zetasizer Nano ZSP, to obtain the hydrodynamic size of the different polymer-coated iron oxide nanoparticles. For that, 100 μL of coated IONPs and 100 μL of distilled water were added to an Eppendorf tube and the nanoparticles were sonicated for 5 to 10 min and measured immediately afterwards in reusable quartz cuvettes.

Atomic absorption spectroscopy (AAS). The device used is a Varian AA140 Atomic Absorption Spectrometer with an acetylene-air flame atomizer. By means of a calibration curve with the iron standard (blank, 0.5, 1, 2, 3, 4, and 5 mg mL^{-1}), and by digesting a known volume of the nanoparticles with 1 mL of aqua regia (overnight), the concentration of the original iron oxide nanoparticles in hexane was obtained ([γ-Fe_2O_3] = 18.8 mg mL^{-1}).

Transmission electron microscopy. Transmission electron microscopy (TEM) imaging was carried out on a FEI-Tecnai G2 F20 microscope, operating at a 200 kV accelerating voltage. The samples were prepared by drop-casting diluted solutions of the iron oxide coated nanoparticles or hydrogel pieces into copper grids, letting the solvent to evaporate under ambient conditions.

Magnetic measurements. The magnetic characterization was performed in a superconducting quantum interference device (SQUID) magnetometer MPMS-3 from Quantum Design. For the measurement of the uncoated iron oxide nanoparticles in hexane and the water transferred polymer coated nanoparticles, 20 μL of the suspension was dropped in a piece of cotton and filled into a glycerin capsule. For the hydrogels, 10 μL of the gels were taken with a pipette and dropped into cotton. Zero field-cooled and field-cooled (ZFC-FC) magnetization curves were measured by applying a magnetic field of 100 Oe from 5 to 300 K. Besides, M–H curves were measured at 5 K and 300 K and a maximum applied field of 5 T. All the measurements were done in DC mode and by using the straw as sample holder, by fixing the sample with cotton inside a gelatin capsule at the right height.

Results and discussion

Nanoparticle characterization and water transfer

The iron oxide nanoparticles have been synthesized following the procedure of Hyeon *et al.*[35] The TEM images of the resulting iron oxide nanoparticles in organic media can be seen in Fig. 1A, along with the size histogram fitted to a log-normal distribution. The nanoparticles are spherical and homogeneous in size, obtaining a narrow size distribution with an average size of 5.0 ± 0.8 nm. The magnetic properties and behavior of the as-synthesized nanoparticles can be seen in Fig. 1B. The superparamagnetic behavior is confirmed, as no coercivity nor remanence occur at 300 K. In addition, the blocking temperature is around 23 K, so the nanoparticles above that temperature are in the superparamagnetic regime. The saturation magnetization at 300 K, M_S = 54 $Am^2\ kg^{-1}$, is below the bulk value (M_{s-bulk} = 80 $Am^2\ kg^{-1}$), which is expected due to the small size of the nanoparticles and the greater influence of the surface, either by the presence of defects or a spin canted or disordered layer.[36,37] As well, it has been reported that when the iron precursor used for the synthesis of the nanoparticles is iron pentacarbonyl, as in this work, the reduction of the magnetic saturation is more pronounced than when using other precursors such as iron acetylacetonate.[38]

These nanoparticles were further coated with amphiphilic polymers, first, to perform the water transfer of the nanoparticles, and then, to force the controlled destabilization to produce the hydrogels *via* the addition of Ca^{2+} ions. The one-pot polymer synthesis allows the obtention of grafted polymers *via*

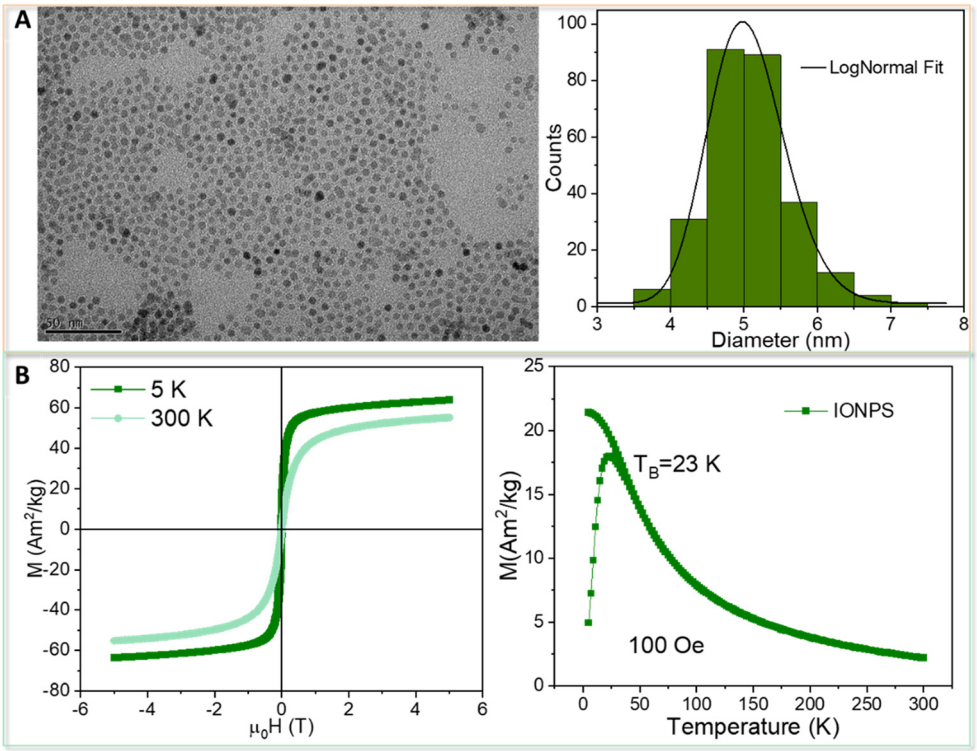

Fig. 1 (A) TEM of the as-synthesized iron oxide nanoparticles and the size distribution fitted to a log-normal and (B) MH curves at 5 K and 300 K and ZFC-FC curves measured applying a magnetic field of 100 Oe.

amide bonding of a hydrophilic backbone, consisting of PMA-poly(isobutylene-*alt*-maleic anhydride), and hydrophobic side-chains. These amphiphilic polymers have proven to be very useful to perform the water transfer of nanoparticles stable in organic media.[26,39,40] The coating of the nanoparticles with amphiphilic polymers and its configuration on the surface of the nanoparticles have been extensively studied.[34,40–42] It has been found that the polymer wraps around the NPs with the hydrophobic side-chains intercalating with the hydrophobic ligands on the surface of the NPs, which are generally assumed to point out of the nanoparticle surface. The nanoparticles are then stable in water due to repulsive electrical forces arising from the negatively charged carboxylate groups from the polymer shell.[26] In this work, two polymers have been synthesized by using two different hydrophobic side-chains with different lengths, dodecylamine and *n*-octylamine, in order to tailor the distances of the magnetic nanoparticles and therefore their interactions when they are part of a gel network (as depicted in Scheme 1). The rationale behind the use of these specific alkyl chain lengths relies in two main aspects: (i) that the ligand is still long enough to be able to attach and wrap around the nanoparticle in the water transfer process and (ii) the ligand length is short enough (octylamine) to observe differences in the magnetic properties between the nanoparticle colloids and their assemblies thereof.

To perform the different coatings, a fixed amount of IONPs in organic media (5.6 mg) was centrifuged and the hexane was exchanged with chloroform (further details in the experimental section). Different amounts of the synthesized polymer PMA-Dod and PMA-Oct, from 100 μL to 3 mL, were mixed with the nanoparticles until complete evaporation of the chloroform. To highlight the versatility of the coating procedure, we have done each of these coatings either by magnetic stirring or ultrasonic bath. DLS measurements have been performed in order to analyze the influence of the polymer amount into the hydrodynamic size of the polymer coated nanoparticles (Fig. 2). The clearest observation is that the use of a shorter alkyl chain produces larger aggregation, and the nanoparticles seem to be closer together, as can be seen in Fig. S1.† TEM of the polymer coated NPs with 100 μL, 400 μL and the scale-up synthesis can be seen in Fig. S1.† The scale-up synthesis procedure can be found in the experimental section. By increasing the amount of polymer, the hydrodynamic size decreases independently of the alkyl chain length used or the procedure used to coat the IONPs (see Fig. 2 and Fig. S2†). Overall, a better coating with less nanoparticle aggregation is reached with higher amounts of polymer. In Table S1,† the amount of monomer per nm^2 can be found for all the samples, values comparable to the one used in our previous work.[26] In the case of dodecylamine, when the amount of polymer is 3 mL, a slight increase in the hydrodynamic size is observed. To go deeper into the understanding on how the coating procedure affects the nanoparticle aggregation, DLS measurements were performed for the samples with smaller amounts of polymer

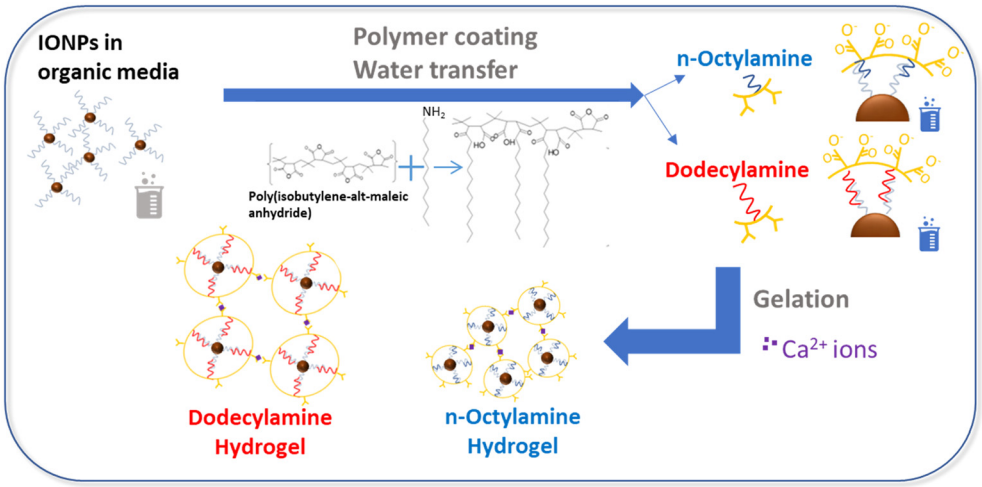

Scheme 1 Polymer coating procedure and resulting hydrogels, highlighting the slightly higher distances expected in the case of coating the nanoparticles with the longer alkyl chains.

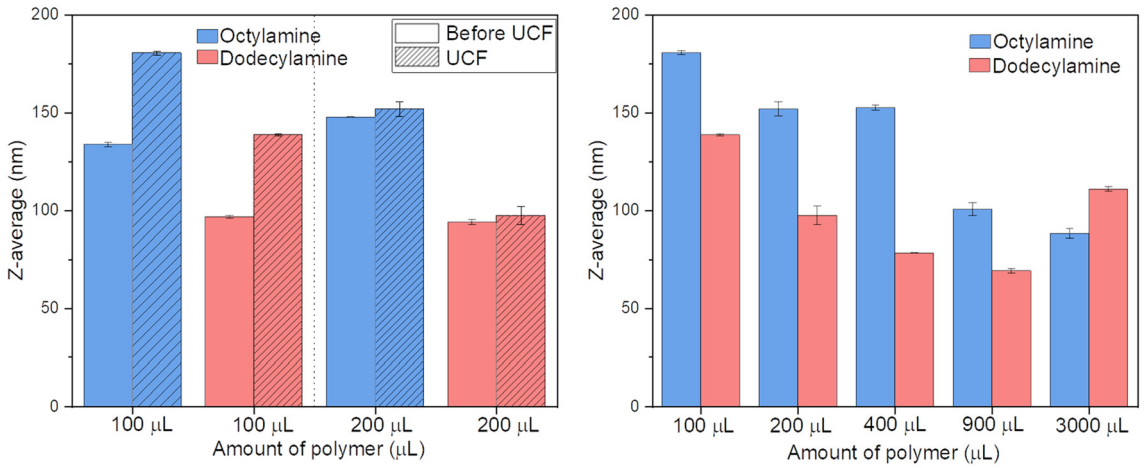

Fig. 2 Hydrodynamic sizes of the polymer-coated NPs (*via* magnetic stirring) measured by DLS, before and after the ultracentrifugation step (left) and of all the samples after ultracentrifugation (right). The error bars represent the standard deviation determined from triplicate DLS measurements.

before and after the ultracentrifugation step, which is used to remove the unreacted polymer micelles. The results show that the high forces to which the nanoparticles are subjected during the ultracentrifugation cause a small aggregation, which is less relevant as the polymer amount increases. For 200 μL of polymer, the difference of the hydrodynamic sizes before and after the ultracentrifugation is reduced, being almost the same. Summarizing, the ultracentrifugation step aggregates more the nanoparticles that are coated with smaller amounts of polymer, which could arise from the partial removal of the polymer which is coating the nanoparticles causing their aggregation.

The scale-up sample was also measured, obtaining a *Z*-average of 117.4 nm, a value close to the one obtained in the case of PMA-Dod coated with 3 mL of polymer. In this sense, we have successfully scaled-up the coating procedure and stable polymer-coated IONPs have been obtained in a large batch, particularly interesting for comparative and optimization studies.

Hydrogels

The hydrogels obtained from the nanoparticles coated either with PMA-Oct or PMA-Dod were obtained *via* the addition of Ca^{2+} ions, which link two adjacent polymer-coated nanoparticles *via* the carboxylate moieties present in the polymer shell.[43] First of all, by the use of the scale-up polymer coated nanoparticles, different amounts of 2 M $Ca(NO_3)_2$ solution were tested to produce the hydrogels. High quality hydrogels can be obtained by using 1 to 8 μL of the Ca^{2+} solution, as can be seen in the TEM images of Fig. S3.† Nevertheless, if the amount is too low, the gels are too fragile and also shrink more than when using a higher amount of gelling agent. For

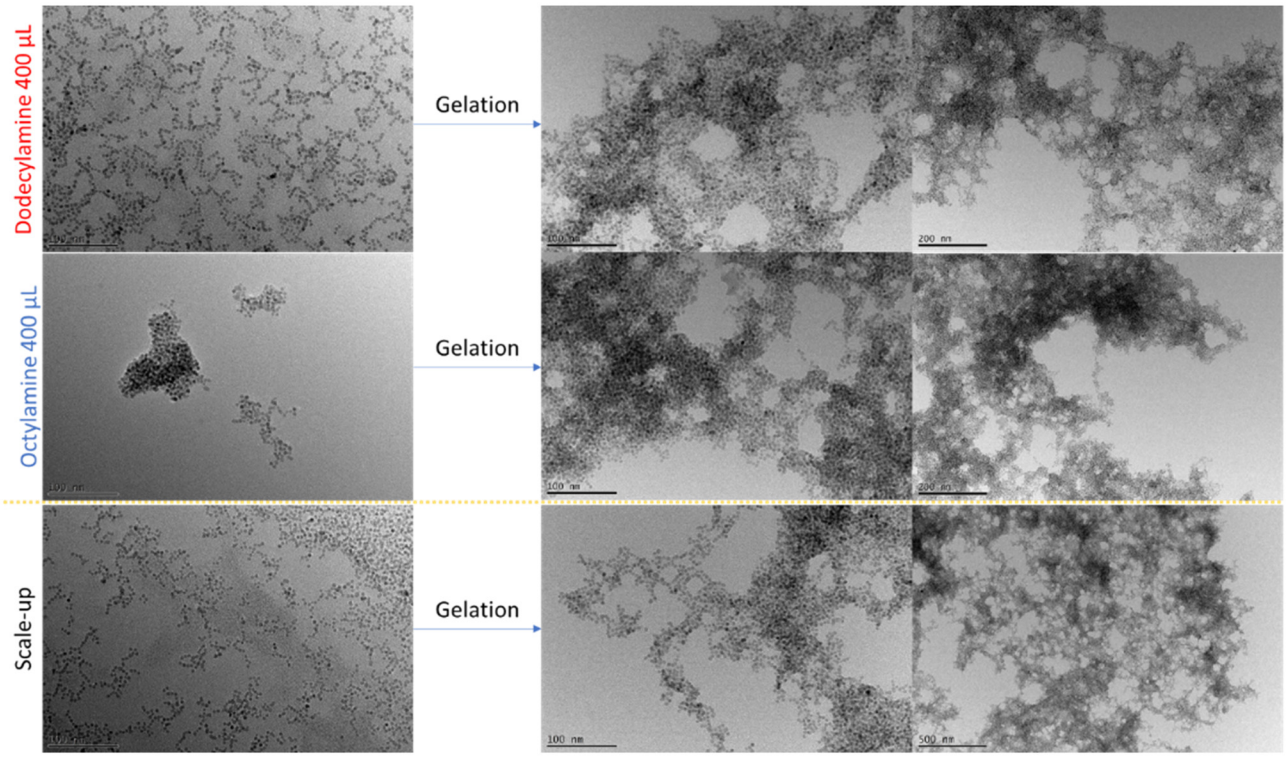

Fig. 3 TEM images of the polymer-coated IONPs and the resulting hydrogels by adding 8 µL of 2 M Ca ions.

all the hydrogels prepared in this work, 8 µL of the 2 M $Ca(NO_3)_2$ solution were used, as the least shrinkage and less fragility was achieved. The TEM of the resulting hydrogels can be seen in Fig. 3. Even if the hydrodynamic size of the PMA-Oct coated nanoparticles is larger in all cases, the resulting hydrogels show a very similar structure as the ones obtained from the PMA-Dod polymer coated nanoparticles and the ones obtained from the scale-up coating approach. No change in the size or the shape occurs to the nanoparticles upon gelation, and no substantial structural differences can be observed between the hydrogels obtained from the nanoparticles coated with PMA-Dod or PMA-Oct. In the TEM it can be seen that the hydrogels obtained in this work show less polymer amount around the nanoparticles and a higher porosity that the ones obtained in our previous work using the same overcoating and gelation procedure.[26] As well, highly porous hydrogels can be obtained by using the ultrasonic bath procedure to coat the nanoparticles (Fig. S4†), demonstrating that the way of coating the nanoparticles is not affecting the nanoparticle properties or the network formation. Therefore, in the following, the work will focus on the magnetic properties of the different polymer-coated NPs and hydrogels obtained from the magnetically stirred IONPs.

Magnetic properties: polymer-coated NP colloids *vs.* hydrogels

To evaluate the magnetic properties and nanoparticle interactions, ZFC-FC measurements have been performed systematically for the polymer coated nanoparticles and the respective hydrogels. The curves have been recorded as follows: (i) the sample was cooled down to 5 K without any applied field, then a small constant field of 100 Oe was applied and the sample was warmed up to 300 K while measuring (ZFC), (ii) the same procedure but the cooling down was done by keeping the applied magnetic field (FC). In superparamagnetic systems, the blocking temperature is given by $T_B = KV/25k_B$,[44,45] where KV is the magnetic anisotropy energy. The magnetic anisotropy energy is defined as the energy barrier which is necessary to overcome to switch the magnetization direction along the easy axis. Initially at low temperatures, the anisotropy barrier is bigger than the thermal energy, and the nanoparticles are in the blocked state. As the temperature increases, the magnetization increases because some nanoparticles have enough energy to overcome the anisotropy barrier and align with the applied magnetic field. The increase continues until reaching the thermodynamic equilibrium, when the magnetization decreases again due to the thermal energy overcoming the anisotropy barrier.[46] When the dipolar interactions between the nanoparticles increase, the blocking temperature increases as well, as a higher temperature is necessary to disorder the magnetic moments of the nanoparticles and reach the superparamagnetic state. Therefore, the evaluation of the blocking temperature is a straightforward way to evaluate magnetic interactions. For the determination of the blocking temperature, the inflection point of the ZFC curve has been taken, as it has been reported that the blocking temperature occurs near this point and it is a better method than by just using the maximum of the ZFC curve.[47]

When the nanoparticles coated with the two different polymers (PMA-Dod and PMA-Oct) are in its colloidal form, the blocking temperature increases with respect to that of the nanoparticles in organic media, but present no consistent correlation with the hydrodynamic sizes and agglomeration of the nanoparticles (Fig. S5†). For example, in the case of using 400 μL of the stock polymer solution for the coating, the hydrodynamic size of the PMA-Oct coated IONPs is higher than for the PMA-Dod IONPs (Fig. 2B), but the blocking temperature of the latter sample is higher, as can be seen in Fig. S5.† Even with a higher agglomeration and by using a shorter alkyl chain, in which the nanoparticles are expected to be closer together, the blocking temperatures are similar or even lower than the ones measured for the IONPs coated with longer alkyl chains. Therefore, the length of the alkyl chain has no clear influence into the dipolar interactions between the nanoparticles in the colloidal form (Fig. S5†), making it difficult to tailor them. Nevertheless, when adding the Ca^{2+} ions, the hydrogels formed with the nanoparticles coated with the shorter alkyl chains present a consistent and systematic increase in the blocking temperature (Fig. 4), and therefore an increased interaction between the particles or aggregates, due to the shorter distance between the NP aggregates within the hydrogel, as depicted in Scheme 1. In Fig. 4C and D, a representative example of the difference in the ZFC-FC curves between the polymer-coated NPs and the hydrogels can be seen, which is observed for all the samples, independently of the amount of polymer used.

The increase in the blocking temperature is only observed in the case of the shorter alkyl chain, independently of the coating procedure or amount of polymer used. The destabilization to form the hydrogels leads to a forced reduction in the

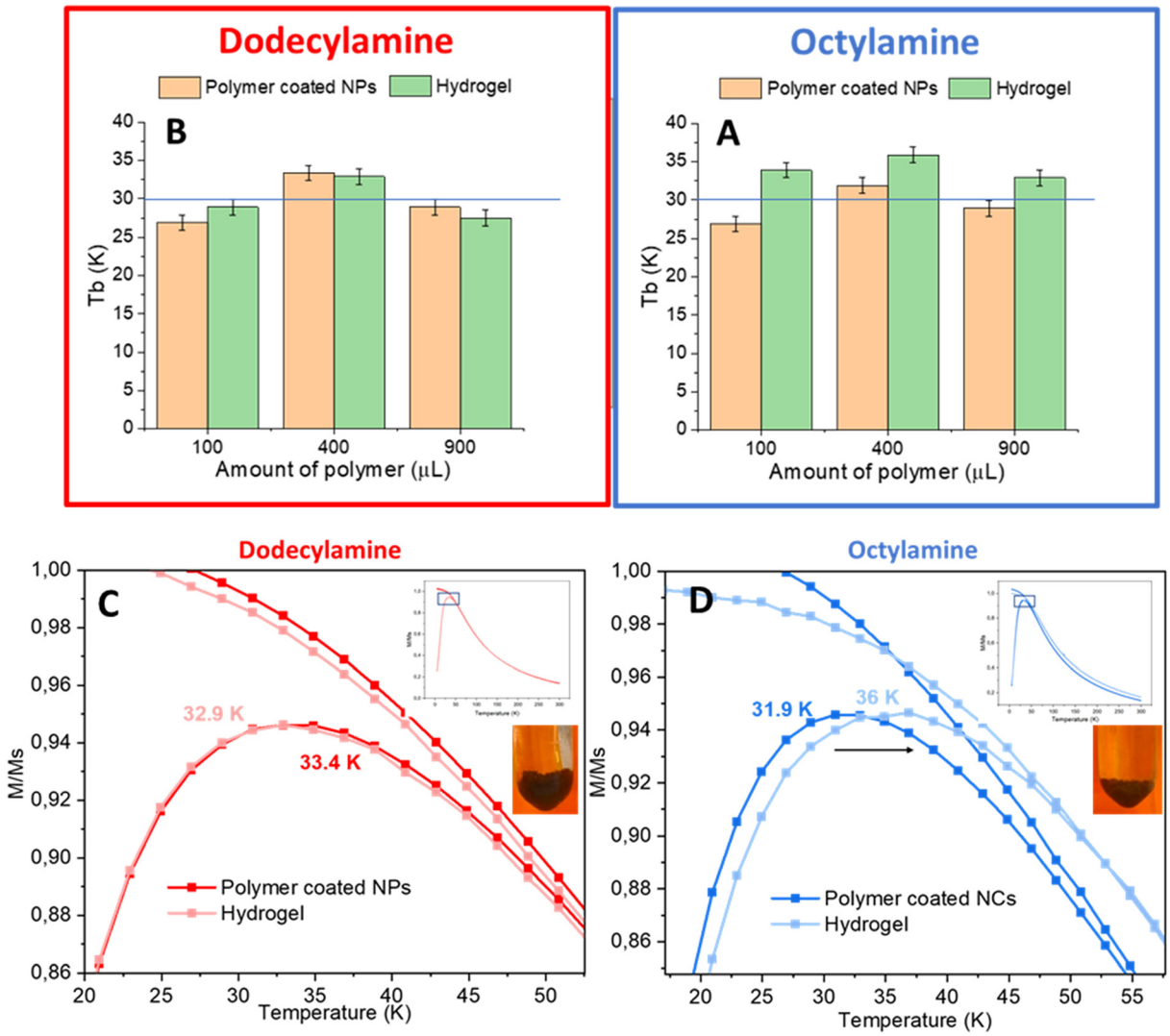

Fig. 4 Summary of the blocking temperatures (T_B) of the polymer-coated IONPs and hydrogels, using octylamine (A) or dodecylamine (B) as side chains. For the calculation of the blocking temperature, the inflection point of the ZFC measured at 100 Oe is taken. ZFC-FC curves of the samples coated with 400 μL of PMA-Dod (C) and PMA-Oct (D), using magnetic stirring to coat the NPs. The values of the blocking temperatures depicted in the image are obtained from the calculation of the inflection point.

distance between the nanoparticles/aggregates, and the small difference between the length of the octylamine and dodecylamine side-chains is enough to see an enhancement in the dipolar interactions when the side-chain length is shorter. The length of the fully extended octylamine is approximately 1.2 nm, while for the dodecylamine is 1.7 nm, according to the values obtained using the Tanford formula,[48] manifesting the small difference in size between both alkyl chains, which nevertheless have an effect in the collective properties of the nanoparticles in the hydrogel. At the same time, it is worth noting that the IONPs average size measured by TEM is around 5 nm, and the difference in length between both alkyl chains represents 10% of the nanoparticle size, so the length difference given the nanoparticle size is significant. An increase in blocking temperature upon gelation indicates an enhancement of magnetic anisotropy due to stronger interparticle interactions within the network for the shorter alkyl chain. These interactions can include dipolar interactions, higher-order magnetostatic interactions or weak exchange interactions, being the latter unlikely due to the nature of the material and the polymer coating. The presence of the magnetic nanoparticles in the self-supported network can give rise to complex magnetostatic fields, which can influence the magnetic behavior of the individual nanoparticles and of the macroscopic system, more pronounced and visible when the nanoparticles are closer and the interactions are stronger (octylamine system).

To further investigate the systems and to have a better insight into the magnetic properties and interactions, the hysteresis cycles have been measured at 5 K and a maximum applied field of 5 T. In particular, the ratio between the remanence and the magnetic saturation ($M_r/M_{s\text{-}5T}$) gives information about the magnetic interactions between the nanoparticles. According to the Stoner–Wolhfarth model,[49] a value of $M_r/M_{s\text{-}5T}$ = 0.5 indicates a system of non-interacting monodomain nanoparticles with the magnetic moments randomly oriented in the remanent state, while deviations of this value account for the kind of interactions occurring. Values of $M_r/M_{s\text{-}5T}$ > 0.5 indicate dipolar interactions between anisotropic assemblies and values of $M_r/M_{s\text{-}5T}$ < 0.5 are observed in systems of isotropically distributed interacting nanoparticles.[50] The normalized hysteresis cycles at 5 K for the polymer coated-nanoparticles and the resulting hydrogels can be seen in Fig. 5. First of all, the ratio $M_r/M_{s\text{-}5T}$ is around 0.2 in all the cases, indicating a system of interacting nanoparticles isotropically distributed. As observed before in the ZFC-FC, the magnetic properties of the nanoparticles coated with the longer alkyl chain (dodecylamine) in the colloid and in the hydrogel are the same.

The ratio $M_r/M_{s\text{-}5T}$ as well as the coercive field remain unchanged, so no increase or decrease in the interactions is observed upon gelation. In the case of the shorter alkyl chain (octylamine), slight differences are observed: a decrease in the $M_r/M_{s\text{-}5T}$ and a small shoulder in the cycle close to 0 Oe of applied magnetic field. On one hand, the reduction of $M_r/M_{s\text{-}5T}$ can be explained by the nanoparticles in the hydrogel being more isotropically distributed than in the colloid, as the distances are fixed by the ligands linked *via* the Ca^{2+} ions. On the other side, interestingly, the shoulder observed could be attributed to two different mechanisms of magnetization inversion, which appear only when the nanoparticles are part of the gel network and when the interparticle interactions are strong enough (not in the case of the dodecylamine as side chain), giving a first hint of collective properties arising in the system.

Summarizing, in the case of the polymer-coated NP colloids, there were no particular differences in the magnetic properties of the nanoparticles coated with PMA-Oct or PMA-Dod (Fig. S5†), being the blocking temperature almost the same independently the alkyl chain length and without correlation

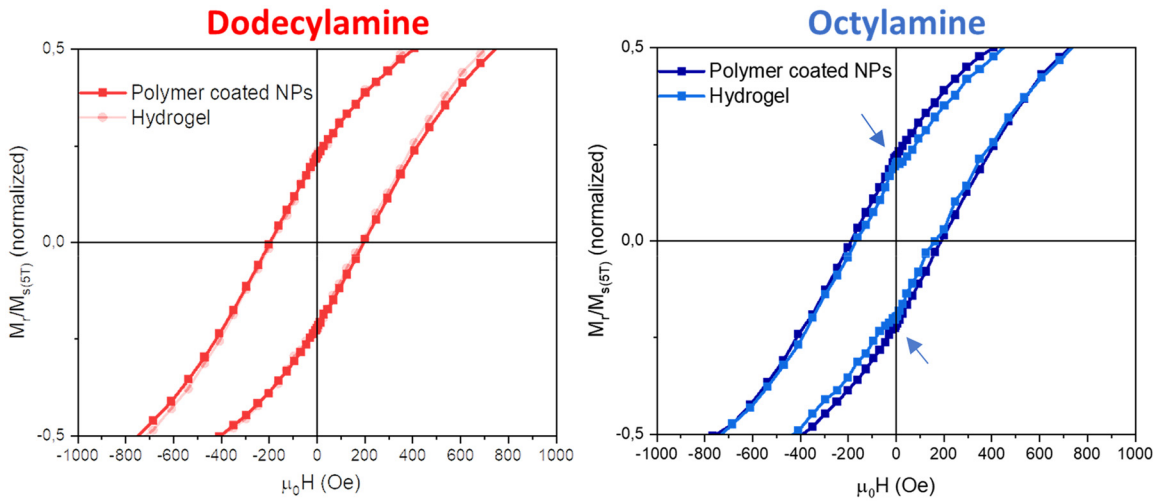

Fig. 5 Hysteresis cycles measured at 5 K for the polymer-coated NPs colloids and the hydrogels obtained from the PMA-Dod (left) and PMA-Oct (right) IONPs (400 μL of polymer stock solution).

to the hydrodynamic size. Nevertheless, when these colloids are destabilized and assembled into hydrogels, only the nanoparticles with shorter alkyl chain showcase a systematic increase in the dipolar interactions, observed through the increase of the blocking temperature. Therefore, we report here a very attractive system in terms of its high porosity and high surface area, and show how to tailor the magnetic properties through the design of the polymer coating procedure and gelation, control which is not directly accessible in the nanoparticle colloids.

Conclusions

In this work we propose for the first time the use of magnetic nanoparticle-based gels as reliable models to go deeper into the study of the magnetic interactions between magnetic nanoparticles and its impact on the overall magnetic properties. Interestingly, differences in the magnetic interactions between the polymer-coated nanoparticles are not clearly observable in the colloids but are systematically observed when the nanoparticles are forced to form the networks building up the gels. For that, the nanoparticles are coated with amphiphilic polymers in which the hydrophobic side chain length is varied and then hydrogels are formed upon the addition of Ca^{2+} ions, observing an increase in the inter-particle or inter-aggregate interactions within the hydrogel when the chain length is shorter and no changes when the length is slightly longer. In the case of the shorter alkyl chain (octylamine), the blocking temperature of the hydrogel increases 4 K on average systematically with respect to the aqueous colloidal nanoparticles, independently of the amount of polymer used to coat the nanoparticles. On the other hand, when using the longer dodecylamine chain, there is no measurable increase or decrease of the interactions between the nanoparticles, being the blocking temperature the same as in its colloidal counterpart. Small differences in the magnetic properties upon aggregation, which in most cases are not expected, can have an undesired influence in different applications such as magnetic hyperthermia. Thus, having a better understanding of these systems is of crucial importance towards the applications of magnetic nanoparticles and hydrogels and to design systems which are more robust against undesired aggregation, as it is the case of the polymer-coated nanoparticles with dodecylamine as side chain.

Data availability

The authors state that the data supporting the results of this study can be found within the paper and its ESI.† If raw data is required, it can be provided by the corresponding author upon reasonable request.

Conflicts of interest

There are no conflicts to declare.

Acknowledgements

This work is supported by the German Research Foundation (Deutsche Forschungsgemeinschaft, DFG) for funding under Germany's excellence strategy within the cluster of excellence PhoenixD (EXC2122, project ID 390833453) and by the Cluster of Excellence CUI: Advanced Imaging of Matter' of the Deutsche Forschungsgemeinschaft (DFG)-EXC2056- project ID 390715994. I. M. acknowledges the support of the Caroline Herschel Program from the Hochschulbüro für Chancenvielfalt, Leibniz University Hannover and the funding by the Cluster of Excellence PhoenixD. R. T. G. thank the Hannover School of Nanotechnology (HSN) for funding. The authors are also thankful for financial support from the German Research Foundation (Deutsche Forschungsgemeinschaft, DFG, Projects BI 1708/4-3 and INST 187/782-1) and to the Laboratory of Nano- and Quantum Engineering (LNQE) for providing the TEM facilities.

References

1 F. Lübkemann-Warwas, I. Morales and N. C. Bigall, *Small Struct.*, 2023, 2300062.
2 C. Ziegler, A. Wolf, W. Liu, A.-K. Herrmann, N. Gaponik and A. Eychmüller, *Angew. Chem., Int. Ed.*, 2017, **56**, 13200–13221.
3 P. Rusch, D. Zámbó and N. C. Bigall, *Acc. Chem. Res.*, 2020, **53**, 2414–2424.
4 A. Eychmüller, *J. Phys. Chem. C*, 2022, **126**, 19011–19023.
5 P. Thoniyot, M. J. Tan, A. A. Karim, D. J. Young and X. J. Loh, *Adv. Sci.*, 2015, **2**, 1400010.
6 L. Korala, J. R. Germain, E. Chen, I. R. Pala, D. Li and S. L. Brock, *Inorg. Chem. Front.*, 2017, **4**, 1451–1457.
7 L. M. Sanchez, D. G. Actis, J. S. Gonzalez, P. M. Zélis and V. A. Alvarez, *J. Nanopart. Res.*, 2019, **21**, 64.
8 S. Sánchez-Paradinas, D. Dorfs, S. Friebe, A. Freytag, A. Wolf and N. C. Bigall, *Adv. Mater.*, 2015, **27**, 6152–6156.
9 D. Pluta, H. Kuper, R. T. Graf, C. Wesemann, P. Rusch, J. A. Becker and N. C. Bigall, *Nanoscale Adv.*, 2023, **5**, 5005–5014.
10 F. Matter, A. L. Luna and M. Niederberger, *Nano Today*, 2020, **30**, 100827.
11 M. Rosebrock, R. T. Graf, D. Kranz, H. Christmann, H. Bronner, A. Hannebauer, D. Zámbó, D. Dorfs and N. C. Bigall, *Small Struct.*, 2023, **4**, 2300186.
12 S. Naskar, A. Freytag, J. Deutsch, N. Wendt, P. Behrens, A. Köckritz and N. C. Bigall, *Chem. Mater.*, 2017, **29**, 9208–9217.
13 M. N. Dominguez, M. P. Howard, J. M. Maier, S. A. Valenzuela, Z. M. Sherman, J. F. Reuther, L. C. Reimnitz, J. Kang, S. H. Cho, S. L. Gibbs, A. K. Menta, D. L. Zhuang, A. van der Stok, S. J. Kline, E. V. Anslyn, T. M. Truskett and D. J. Milliron, *Chem. Mater.*, 2020, **32**, 10235–10245.
14 F. J. Heiligtag, M. J. A. Leccardi, D. Erdem, M. J. Süess and M. Niederberger, *Nanoscale*, 2014, **6**, 13213–13221.

15 L. Xue and J. Sun, *Front. Chem.*, 2022, **10**, 1040492.
16 N. Shah, T. Rehan, X. Li, H. Tetik, G. Yang, K. Zhao and D. Lin, *RSC Adv.*, 2021, **11**, 7187–7204.
17 S. Ganguly and S. Margel, *Prog. Polym. Sci.*, 2022, **131**, 101574.
18 J. Tang, Q. Yin, M. Shi, M. Yang, H. Yang, B. Sun, B. Guo and T. Wang, *Extreme Mech. Lett.*, 2021, **46**, 101305.
19 N. Singh, S. Riyajuddin, K. Ghosh, S. K. Mehta and A. Dan, *ACS Appl. Nano Mater.*, 2019, **2**, 7379–7392.
20 R. Weeber, P. Kreissl and C. Holm, *Phys. Sci. Rev.*, 2023, **8**, 1465–1486.
21 M. A. Hettiarachchi, T. Su'a, A. Ramzan, S. Pokhrel, B. Nadgorny and S. L. Brock, *J. Phys. Chem. C*, 2022, **126**, 2088–2097.
22 T. Berestok, J. Chacón-Borrero, J. Li, P. Guardia and A. Cabot, *Langmuir*, 2023, **39**, 3692–3698.
23 E. I. Anastasova, V. Ivanovski, A. F. Fakhardo, A. I. Lepeshkin, S. Omar, A. S. Drozdov and V. V. Vinogradov, *Soft Matter*, 2017, **13**, 8651–8660.
24 L. Schoske, F. Lübkemann-Warwas, I. Morales, C. Wesemann, J. G. Eckert, R. T. Graf and N. C. Bigall, *Nanoscale*, 2024, **16**, 4229–4238.
25 N. Ganonyan, J. He, A. Temkin, I. Felner, R. Gvishi and D. Avnir, *Appl. Mater. Today*, 2021, **22**, 100955.
26 L. Altenschmidt, S. Sánchez-Paradinas, F. Lübkemann, D. Zámbó, A. M. Abdelmonem, H. Bradtmüller, A. Masood, I. Morales, P. de la Presa, A. Knebel, M. A. G. García-Tuñón, B. Pelaz, K. D. J. Hindricks, P. Behrens, W. J. Parak and N. C. Bigall, *ACS Appl. Nano Mater.*, 2021, **4**, 6678–6688.
27 E. H. Sánchez, M. Vasilakaki, S. S. Lee, P. S. Normile, M. S. Andersson, R. Mathieu, A. López-Ortega, B. P. Pichon, D. Peddis, C. Binns, P. Nordblad, K. Trohidou, J. Nogués and J. A. De Toro, *Small*, 2022, **18**, 2106762.
28 J. A. De Toro, P. S. Normile, S. S. Lee, D. Salazar, J. L. Cheong, P. Muñiz, J. M. Riveiro, M. Hillenkamp, F. Tournus, A. Tamion and P. Nordblad, *J. Phys. Chem. C*, 2013, **117**, 10213–10219.
29 A. S. Eggeman, S. A. Majetich, D. Farrell and Q. A. Pankhurst, *IEEE Trans. Magn.*, 2007, **43**, 2451–2453.
30 R. Fu, Y. Yan, C. Roberts, Z. Liu and Y. Chen, *Sci. Rep.*, 2018, **8**, 4704.
31 J. G. Ovejero, D. Cabrera, J. Carrey, T. Valdivielso, G. Salas and F. J. Teran, *Phys. Chem. Chem. Phys.*, 2016, **18**, 10954–10963.
32 P. De La Presa, Y. Luengo, V. Velasco, M. P. Morales, M. Iglesias, S. Veintemillas-Verdaguer, P. Crespo and A. Hernando, *J. Phys. Chem. C*, 2015, **119**, 11022–11030.
33 J. Mohapatra, S. Nigam, J. Gupta, A. Mitra, M. Aslam and D. Bahadur, *RSC Adv.*, 2015, **5**, 14311–14321.
34 C.-A. J. Lin, R. A. Sperling, J. K. Li, T.-Y. Yang, P.-Y. Li, M. Zanella, W. H. Chang and W. J. Parak, *Small*, 2008, **4**, 334–341.
35 T. Hyeon, S. S. Lee, J. Park, Y. Chung and H. B. Na, *J. Am. Chem. Soc.*, 2001, **123**, 12798–12801.
36 W. Baaziz, B. P. Pichon, S. Fleutot, Y. Liu, C. Lefevre, J.-M. Greneche, M. Toumi, T. Mhiri and S. Begin-Colin, *J. Phys. Chem. C*, 2014, **118**, 3795–3810.
37 Z. Nedelkoski, D. Kepaptsoglou, L. Lari, T. Wen, R. A. Booth, S. D. Oberdick, P. L. Galindo, Q. M. Ramasse, R. F. L. Evans, S. Majetich and V. K. Lazarov, *Sci. Rep.*, 2017, **7**, 45997.
38 A. Lak, S. Disch and P. Bender, *Adv. Sci.*, 2021, **8**, 2002682.
39 S. K. Yen, D. Jańczewski, J. L. Lakshmi, S. B. Dolmanan, S. Tripathy, V. H. B. Ho, V. Vijayaragavan, A. Hariharan, P. Padmanabhan, K. K. Bhakoo, T. Sudhaharan, S. Ahmed, Y. Zhang and S. Tamil Selvan, *ACS Nano*, 2013, **7**, 6796–6805.
40 A. M. Abdelmonem, A. Lavrentieva and N. C. Bigall, *Chem. Pap.*, 2024, **78**, 533–546.
41 T. Pellegrino, L. Manna, S. Kudera, T. Liedl, D. Koktysh, A. L. Rogach, S. Keller, J. Rädler, G. Natile and W. J. Parak, *Nano Lett.*, 2004, **4**, 703–707.
42 W. W. Yu, E. Chang, J. C. Falkner, J. Zhang, A. M. Al-Somali, C. M. Sayes, J. Johns, R. Drezek and V. L. Colvin, *J. Am. Chem. Soc.*, 2007, **129**, 2871–2879.
43 D. Wen, A.-K. Herrmann, L. Borchardt, F. Simon, W. Liu, S. Kaskel and A. Eychmüller, *J. Am. Chem. Soc.*, 2014, **136**, 2727–2730.
44 H. K. D. Kim, L. T. Schelhas, S. Keller, J. L. Hockel, S. H. Tolbert and G. P. Carman, *Nano Lett.*, 2013, **13**, 884–888.
45 M. Knobel, W. C. Nunes, L. M. Socolovsky, E. De Biasi, J. M. Vargas and J. C. Denardin, *J. Nanosci. Nanotechnol.*, 2008, **8**, 2836–2857.
46 I. J. Bruvera, P. Mendoza Zélis, M. Pilar Calatayud, G. F. Goya and F. H. Sánchez, *J. Appl. Phys.*, 2015, **118**, 184304.
47 K. L. Livesey, S. Ruta, N. R. Anderson, D. Baldomir, R. W. Chantrell and D. Serantes, *Sci. Rep.*, 2018, **8**, 11166.
48 C. Tanford, *J. Phys. Chem.*, 1972, **76**, 3020–3024.
49 E. C. Stoner and E. P. Wohlfarth, *Philos. Trans. R. Soc. London, Ser. A*, 1948, **240**, 599–642.
50 B. Mehdaoui, R. P. Tan, A. Meffre, J. Carrey, S. Lachaize, B. Chaudret and M. Respaud, *Phys. Rev. B:Condens. Matter Mater. Phys.*, 2013, **87**, 174419.